Neuromorphic Dynamical Synapses With Reconfigurable Voltage-Gated Kinetics

Jun Wang, Gert Cauwenberghs, *Fellow, IEEE*, and Frédéric D. Broccard

Abstract*—*Objective: **Although biological synapses express a large variety of receptors in neuronal membranes, the current hardware implementation of neuromorphic synapses often rely on simple models ignoring the heterogeneity of synaptic transmission. Our objective is to emulate different types of synapses with distinct properties.** ***Methods:*** **Conductance-based chemical and electrical synapses were implemented between silicon neurons on a fully programmable and reconfigurable, biophysically realistic neuromorphic VLSI chip. Different synaptic properties were achieved by configuring on-chip digital parameters for the conductances, reversal potentials, and voltage dependence of the channel kinetics. The measured I-V characteristics of the artificial synapses were compared with biological data.** ***Results:*** **We reproduced the response properties of five different types of chemical synapses, including both excitatory ($AMPA$, $NMDA$) and inhibitory ($GABA_A$, $GABA_C$, $glycine$) ionotropic receptors. In addition, electrical synapses were implemented in a small network of four silicon neurons.** ***Conclusion:*** **Our work extends the repertoire of synapse types between silicon neurons, providing greater flexibility for the design and implementation of biologically realistic neural networks on neuromorphic chips.** ***Significance:*** **A higher synaptic heterogeneity in neuromorphic chips is relevant for the hardware implementation of energy-efficient population codes as well as for dynamic clamp applications where neural models are implemented in neuromorphic VLSI hardware.**

***Index Terms*—Neuromorphic engineering, silicon neuron, chemical synapse, electrical synapse, biohybrid circuits, reconfigurable VLSI.**

I. Introduction

IN BOTH vertebrates and invertebrates, synapses are the fundamental computational elements of nervous systems enabling communication and information processing at spatial and temporal scales spanning over several orders of magnitude [3]. Synapses are highly diverse and use two main modalities of transmission: electrical and chemical. In electrical synapses, the cytoplasm of adjacent neurons is directly connected by intracellular channels called gap junctions, allowing the exchange of small molecules (e.g. Ca^{2+}, cAMP, IP3) and electrical potentials [4], [5]. The strength of electrical synapses depends on the graded transsynaptic voltage difference, thus providing bidirectional and analogical communication among adjacent neurons. In chemical synapses, neurotransmitter molecules released at the presynaptic site diffuse across the synaptic cleft and activate postsynaptic receptors. Chemical synapses are predominant in vertebrates and exhibit a vast diversity of sub-types with high molecular heterogeneity [6], [7] and large functional differences in individual properties expressed both at the pre- and postsynaptic sites. At the presynaptic site, the molecular heterogeneity is exemplified by the large variety of neurotransmitters present in synaptic vesicles, including amino acids, monoamines, peptides, purines, gaseous molecules, and other molecules such as acetylcholine [8]. At the postsynaptic site, the types of receptor show a corresponding diversity with several different sub-types of receptors for a given neurotransmitter, each of these subtypes existing in various forms depending on the composition and past molecular modifications of their individual sub-units. Taken together, the heterogeneity of mechanisms involved in synaptic transmission (and their plasticity) is thought to underlie the complex adaptive and multistable dynamics of neurons [7], [9]. At the network level, recent theoretical analysis and computational works suggest that the heterogeneity of neuron and synapse types reduces the cost of computation [10], [11], and enables the implementation of energy-efficient population codes [12]–[14].

In mixed analog-digital neuromorphic VLSI systems, the electronic circuits of silicon neurons and synapses exhibit an inherent structural heterogeneity due to device mismatch, noise, and temperature sensitivity during fabrication processes [15]. However, the functional diversity of synapse types remains largely unexplored, and most of the neural network models implemented on mixed analog-digital neuromorphic hardware typically implement one type of excitatory –and one type of inhibitory– synapse [16]. The small number of synapse types emulated on hardware also severely limits the range of dynamic clamp applications using neural models implemented on neuromorphic chips [17], [18].

This paper presents theory and experimental validation of biophysically realistic synapses implemented on *NeuroDyn*, a fully

Manuscript received July 5, 2019; revised September 16, 2019; accepted October 10, 2019. Date of publication October 22, 2019; date of current version June 18, 2020. This work was supported in part by the Office of Naval Research in part by the National Science Foundation the University of California Multicampus Research Programs and Initiatives, Intel Corporation, Fujitsu, and Texas Instruments. *(Corresponding author: Frédéric D. Broccard.)*

J. Wang is with the Department of Bioengineering and the Center for Engineered Natural Intelligence, University of California San Diego.

G. Cauwenberghs is with the Department of Bioengineering, the Center for Engineered Natural Intelligence, and the Institute for Neural Computation, UC San Diego.

F. D. Broccard is with the Department of Bioengineering and the Institute for Neural Computation, University of California San Diego, La Jolla, CA 92093 USA (e-mail: fbroccard@ucsd.edu).

Digital Object Identifier 10.1109/TBME.2019.2948809

0018-9294 © 2019 IEEE. Personal use is permitted, but republication/redistribution requires IEEE permission.
See https://www.ieee.org/publications/rights/index.html for more information.

Authorized licensed use limited to: Univ of Calif San Diego. Downloaded on August 06,2021 at 09:57:53 UTC from IEEE Xplore. Restrictions apply.

programmable and reconfigurable neuromorphic VLSI chip [1], [2]. Here we offer a complete characterization of a wide range of different types of synapses, extending on initial characterization reported in [19], by including excitatory and inhibitory chemical synapses mediated by ionotropic receptors, as well as electrical synapses mediated by gap junctions.

The remainder of this paper is organized as follows. Section II details the implementation of the reconfigurable biophysical electrochemical synapses, and Section III describes their characterization with measured data including the mapping of dynamical response characteristics for synapses with excitatory (AMPA and NMDA) and inhibitory ($\mathrm{GABA_A}$, $\mathrm{GABA_C}$, Glycine) receptors. The characterization of electrical synapses is presented in Section IV. Finally, discussion and concluding remarks are presented in Sections V and VI, respectively.

II. Synapse Implementation

Chemical and electrical synapses were implemented on a fully programmable and reconfigurable, biophysically realistic neuromorphic VLSI chip, *NeuroDyn* (Fig. 1), of which the neuronal soma dynamics was previously detailed in [1], [2]. Briefly, the *NeuroDyn* chip consists of four Hodgkin-Huxley (HH) neurons N_i $(i = 1, \ldots 4)$ connected by twelve conductance-based synapses W_{ij} $(j = 1, \ldots 4; j \neq i)$ for a total of 384 digitally programmable parameters governing the channel conductances, reverse potentials, and voltage dependence of the channel kinetics (opening and closing rates). The 12 synapses are governed by half of the 384 parameters. Namely, each synapse has 16 parameters. The other half of the parameters governs the individual dynamics of the 4 neurons. The *NeuroDyn* chip measures 3 mm $\times$ 3 mm in 0.5 μm CMOS and consumes 1.29 mW static power. A detailed description of the *NeuroDyn* parameters and VLSI implementation is described in [1].

The HH dynamics in membrane potential V_{mem} for each of the neurons N_i is described by

$$C_{mem}\frac{dV_{mem}}{dt} = -I_{Na} - I_K - I_L + I_{Inj} + I_{Syn} \quad (1)$$

where C_{mem} is the membrane capacitance, I_{Na}, I_K and I_L represent the sodium, potassium, and leak conductance-based currents, respectively, I_{Inj} is the injected current, and I_{Syn} is the net synaptic current as contributed by the other three neurons N_j, $j \neq i$. By default *NeuroDyn* implements chemical synapses, which however can further be configured to function as electrical synapses (Sec. IV). In the default chemical synapse mode of operation, each of the three conductance-based synaptic currents is modeled as

$$I_{Syn}(t) = g_{syn}\; r(t)\; (V_{post}(t) - E_{syn}) \quad (2)$$

through a single rate-based kinetic variable $r(t)$ governed by V_{pre}. The presynaptic potential V_{pre} induces release of neurotransmitter that binds with receptors on the postsynaptic site to activate the conductance on the postsynaptic membrane V_{post} with reversal potential E_{syn}. Similarly to the other channel gating variables, the dynamics of the synaptic variable r, the fraction of receptors in the open state, is described by first-order

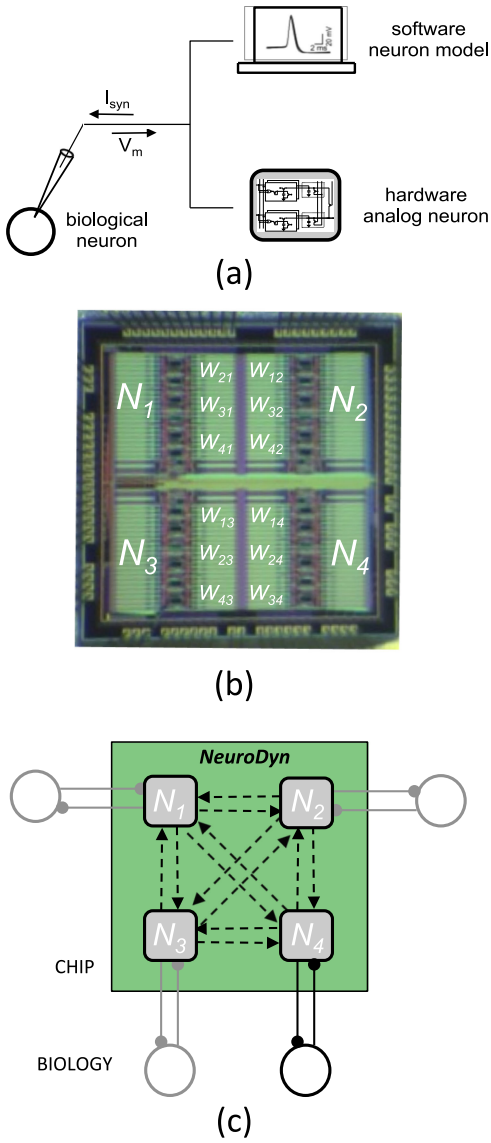

Fig. 1. Neuromorphic dynamic clamp. (a) Dynamic clamp protocol with neural models implemented in digital software or analog hardware. (b) Micrograph of the *NeuroDyn* chip with four silicon neurons [1], [2] (Sec. II). (c) Simultaneous dynamic clamp with multiple reconfigurable silicon neurons.

kinetics through the usual rate equation:

$$\frac{dr}{dt} = \alpha_r(V_{pre})\;(1 - r) - \beta_r(V_{post})\;r \quad (3)$$

where the opening rate α_r depends on the presynaptic membrane voltage V_{pre} and the closing rate β_r depends on the postsynaptic membrane voltage V_{post}. Hence $\alpha_r(V_{pre})$ models activation of postsynaptic conductance triggered by a presynaptic action potential, and $\beta_r(V_{post})$ models relaxation of the conductance which particularly for the NMDA synapse type is strongly dependent on postsynaptic potential, giving rise to nonlinear dynamics. Like the rates for the other kinetic variables m, n and h that modulate cell excitability in *NeuroDyn* [1], [2], the opening α_r and closing β_r rates for the synapse kinetic variables are modeled and regressed as 7-point additive spline sigmoidal

Authorized licensed use limited to: Univ of Calif San Diego. Downloaded on August 06,2021 at 09:57:53 UTC from IEEE Xplore. Restrictions apply.

functions:

$$\alpha_r(V_{pre}) = \sum_{k=1}^{7} \alpha_{r,k}\ \sigma_k(V_{pre}) \tag{4}$$

$$\beta_r(V_{post}) = \sum_{k=1}^{7} \beta_{r,k}\ \sigma_k(V_{post}) \tag{5}$$

with fixed sigmoids

$$\sigma_k(V) = \frac{1}{1 + e^{\pm\mu(V_{b,k} - V)}} \tag{6}$$

at uniformly spaced centers spanning the voltage range

$$V_{b,k} = V_{b,min} + \frac{k-1}{6}(V_{b,max} - V_{b,min}). \tag{7}$$

As such, $\alpha_{r,k}$, $\beta_{r,k}$,$V_{b,min}$ and $V_{b,max}$ are programmable parameters that allow control over the temporal characteristics of individual synapses, emulating various dynamical synapse types. The polarity ($\pm$) in the exponent in Eqn. (6) is programmed as either $+1$ or -1 through an additional binary parameter for each α_r and β_r, supporting either a monotonically increasing or a monotonically decreasing voltage profile for each of the opening and closing rates.

These parameters govern the voltage-dependent profile of α_r and β_r and thereby determine the voltage-dependent time constant and asymptote of synaptic variables r that can be tuned to observed time constants and asymptote from patch clamp cellular recordings of synaptic function. *NeuroDyn* provides two means of user control over these parameters: *i)* global biasing to uniformly scale all currents $\alpha_{r,k}$, $\beta_{r,k}$ by a current reference I_{ref} and, independently, a voltage reference $V_{ref} = V_{b,max} - V_{b,min}$; and *ii)* individual digital programming of each of these parameters relative to these reference scales. *NeuroDyn* supports operation over a wide range of these scales to allow reaching biologically consistent ranges of conductances and time constants, although in this work we have fixed these ranges at larger current and voltage scales for convenience in the measurements accommodating dynamic range above instrumentation noise and below saturation levels. Digital programming accommodates 12 bits of resolution in each of the parameters. The sensitivity of the spline function parameters $\alpha_{r,k}$ and $\beta_{r,k}$ depend on the range of the membrane voltage V_{mem} and are greatest near their respective bias point $V_{b,k}$.

We tuned the parameters governing neuromorphic synapses to fit the published data describing the kinetic properties of several ionotropic receptors and gap junctions present in biological synapses. The particular functional form of *NeuroDyn* postsynaptic dynamics, with strictly monotonic opening and closing rates in presynaptic and postsynaptic potential, respectively, limit the approximation quality of general nonlinear dynamics in postsynaptic conductance that can be realized, although we were able to generate distinct dynamics specific to different biological synapse types. For proof-of-concept we performed manual parameter tuning; more systematic methods can be applied for automated tuning of parameters through data assimilation [21] but require explicit data on internal dynamics of at least a subset of the state variables in response to specific stimulus sequences, which are not available here. In particular, we performed an initial manual parameter sweep in order to identify suitable regions of the parameter space. We then used a relatively simple calibration and parameter fitting procedure by tuning each of the internal variables in the dynamics in isolation based on detailed model knowledge and applying rectified linear regression and iterative linear least-squares residue correction as described in detail in [1]. This method proved adequate to compensate for device mismatch and to set parameters in the biophysical model approximately to desired values [1].

III. Chemical Synapses

To characterize the different chemical synapses, two silicon neurons were randomly selected from the *NeuroDyn* chip and assigned as pre- and postsynaptic neuron, respectively. The presynaptic neuron was then stimulated with an electrical pulse of 20 mV for 2000 ms (pulse width = 1000 ms) that mimicked the neurotransmitter release and triggered a current flow into the postsynaptic neuron. These parameters were chosen based on convenience of recording but could be set to smaller or larger values. The postsynaptic neuron had its potential clamped in order to measure the whole-cell current which simulated the response of the ionotropic receptors. The stimulation of the presynaptic neuron and the recording of the postsynaptic receptor responses were achieved with two Keithley source meters (Tektronics, El Cajon, CA). Currents and voltages were measured from peripheral pads of the *NeuroDyn*'s supporting PCB board. The membrane potentials of both the pre- and postsynaptic neurons were recorded with an oscilloscope (Agilent Technologies, La Jolla, CA) and saved with a custom Matlab script (The MathWorks, Inc., Natick, MA) for off-line analysis. The responses of five different common ionotropic receptors present in both excitatory (AMPA, NMDA) and inhibitory ($\mathrm{GABA_A}$, $\mathrm{GABA_C}$ and Glycine) synapses were obtained by configuring the *NeuroDyn* on-chip digital parameters for the synaptic reversal potentials, conductance, and opening and closing rate voltage splines. The measured I-V characteristics of the five types of ionotropic receptors were compared with biological data published in the literature.

A. AMPA and NMDA Receptors

The amino acid glutamate mediates most of the excitatory synaptic transmission in the central nervous system and spinal cord. Glutamate binds and activates three families of cation permeable ligand-gated receptors, including the α-amino3-hydroxy-5-methyl-isoxazolepropionic acid (AMPA) receptors, the N-methyl-D-aspartate (NMDA) receptors, and kainate receptrors. All three families of ionotropic glutamate receptors play essential roles in synaptic plasticity. The different affinity of these families of receptors for glutamate, their different activation/deactivation kinetics, and ionic selectivity have all important functional consequences.

AMPA receptors are highly permeable to $\mathrm{Na^+}$ ions, have a low affinity for glutamate, and a fast kinetics ensuring a rapid depolarization of the neuronal membrane. As AMPA receptors with different sub-unit composition display a wide range of

Authorized licensed use limited to: Univ of Calif San Diego. Downloaded on August 06,2021 at 09:57:53 UTC from IEEE Xplore. Restrictions apply.

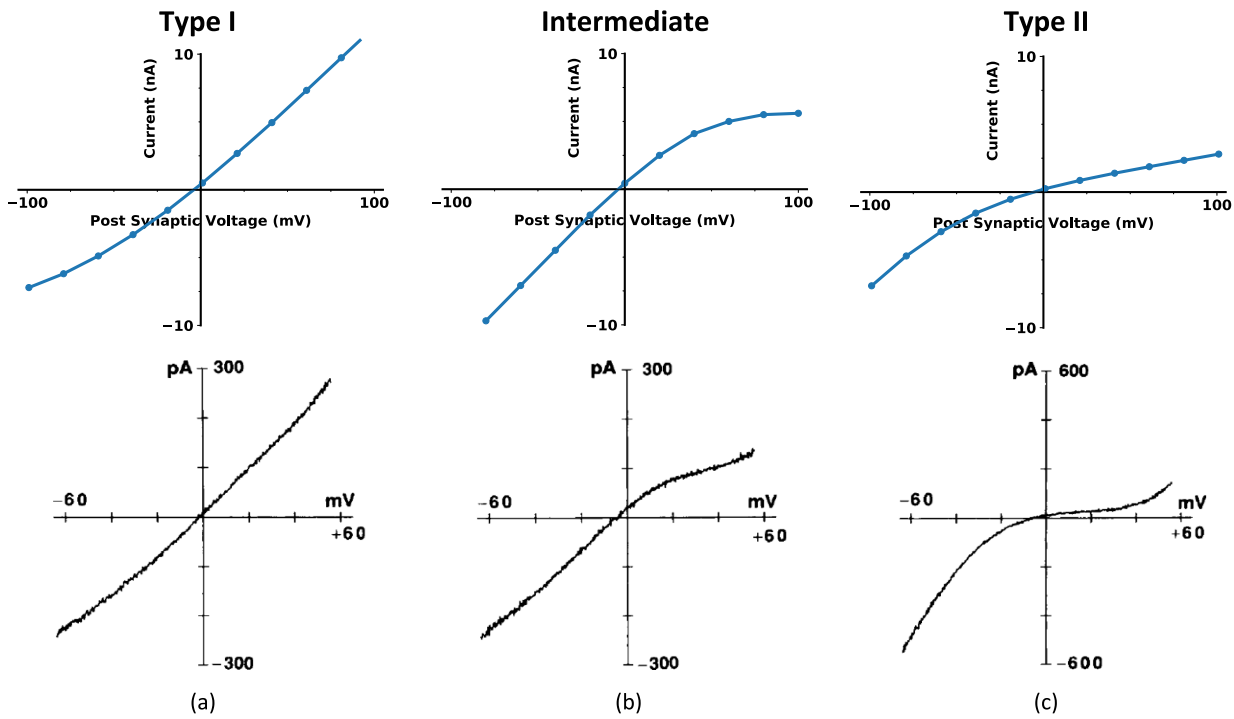

Fig. 2. Characterization of the AMPA receptor responses. *Top, NeuroDyn* measurements of three different I-V relations exhibited by different receptor subtypes (a-c), from outward (Type I) to slight (intermediate) and pronounced inward rectification (Type II), as observed in rat neocortical neurons (*bottom*) [20]. Discrepancies in the mapping are mostly due to the functional form of *NeuroDyn* limited to strictly monotonic slopes in nonlinear postsynaptic conductance. The scale of the *NeuroDyn* currents is adjustable, and shown here is larger than biophysical for faster-than-real time in the emulated dynamics.

rectification properties, we emulated AMPA receptors exhibiting either inward or outward rectification (Fig. 2), as described for native and other common variation of AMPA receptors, respectively [20], [23]. Stimulation from presynaptic neurons were mimicked by a 20 mV electrical pulse with a pulse width of 1000 ms while the current in the postsynaptic neuron was recorded in voltage-clamp mode.

In contrast to AMPA receptors, NMDA receptors have unique biophysical properties including a high permeability to Ca^{2+} ions, a high unitary conductance, a voltage-sensitive block by extracellular Mg^{2+}, and a slower activation/deactivation kinetics. NMDA receptors also have a higher affinity for glutamate than AMPA receptors. The different glutamate affinity and kinetics of AMPA and NMDA receptors have important functional consequences in central synapses where both receptor types are often co-localized; the rapid activation of AMPA receptors elicits a quick depolarization of the neuronal membrane that relieves NMDA receptors from their voltage-sensitive Mg^{2+} blockade. The effect of the Mg^{2+} blockade limiting the conductance of an NMDA synapse is shown in Fig. 3a. The voltage-sensitive Mg^{2+} blockade and resulting outward rectification are shown in Fig. 3b. In that case, the value of the reverse potential was 0 mV. Changes in the Mg^{2+} concentration were triggered by applying a step function to the presynaptic voltage (V_{pre}). We also studied the divalent cation permeability of the NMDA receptors by mimicking a change in the extracellular ionic composition, as shown originally in cultured neurons [24] and recombined heteromeric receptors [22]. Changing the extracellular Na^{+} ions by Ca^{2+} ions resulted in a 20 mV shift of the reversal potential, from 0 to 20 mV, respectively (Fig. 3c). This was achieved by changing the value of the synaptic reversal potential, E_{syn}, from 0 to 20 mV, and adjusting the maximum conductance g_{syn} (Eqn. (2)). This effect of Mg^{2+} changing the current flow into the postsynaptic neuron is mediated by the postsynaptic membrane potential, as modeled here through the dependence of the closing rate β_r on the postsynaptic potential V_{post} (Eqn. (5)). Based on this assumption, we conducted experiments to demonstrate the effect of the NMDA synapse on neuronal spiking patterns. The results are shown in Fig. 4. After 'adding Mg^{2+}' by changing the governing parameters, the postsynaptic neuron was triggered to spike.

B. $GABA_A$ and $GABA_C$ Receptors

Next, we implemented inhibitory chemical synapses for the γ-aminobutyric acid (GABA), the major inhibitory neurotransmitter in the central nervous system [25], [26]. GABA acts on two types of ionotropic receptors, $\mathrm{GABA_A}$ and $\mathrm{GABA_C}$, and one type of metabotropic receptor, $\mathrm{GABA_B}$. $\mathrm{GABA_A}$ and $\mathrm{GABA_C}$ receptors have different pharmacological properties, different single channel conductances while retaining similar kinetics and permeability to chloride ions. Following GABA release, $\mathrm{GABA_A}$ receptors are responsible for the transient component of the GABA response, whereas $\mathrm{GABA_C}$ receptors mediates a more sustained response [27]. To further demonstrate the versatility of the *NeuroDyn* chip, we emulated the synapses

Authorized licensed use limited to: Univ of Calif San Diego. Downloaded on August 06,2021 at 09:57:53 UTC from IEEE Xplore. Restrictions apply.

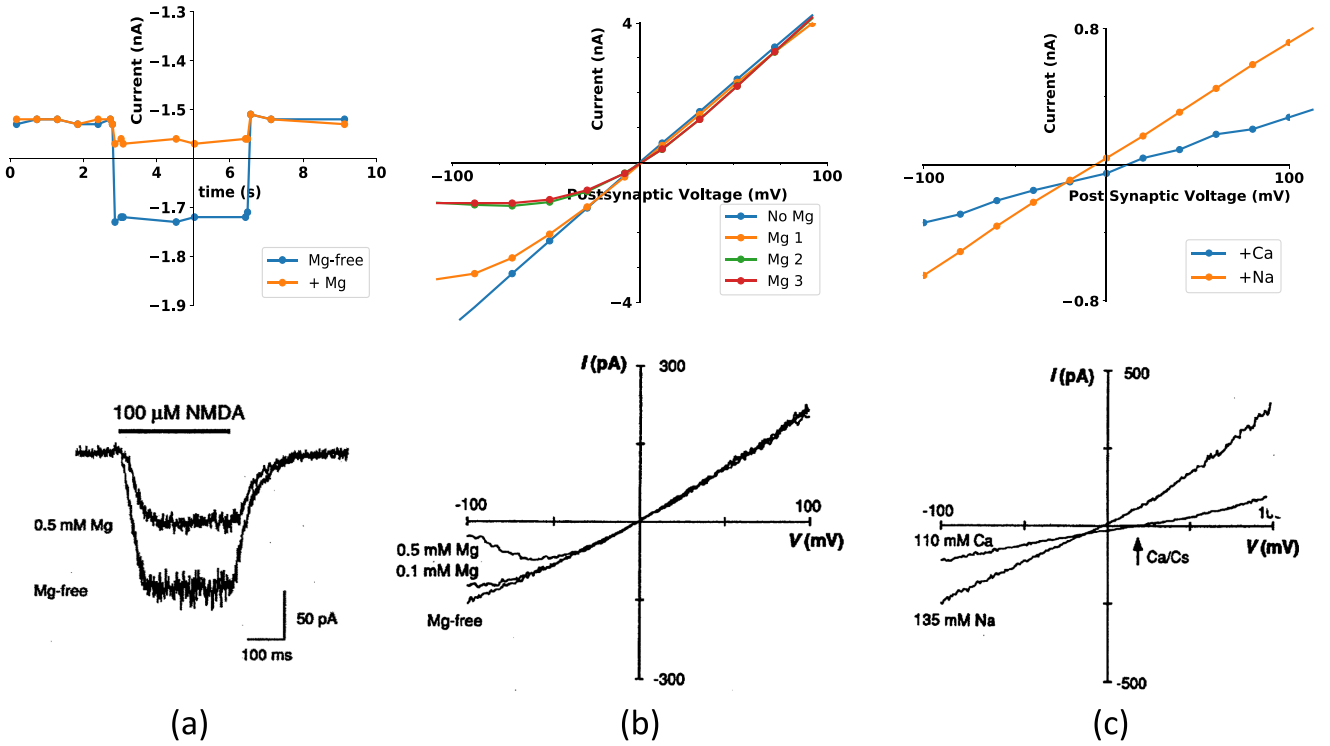

Fig. 3. NMDA receptor characterization by emulating the conductance and ion permeability properties of NMDA receptor channels. *Top*: *NeuroDyn* measurements; *Bottom*: electrophysiological recordings adapted from [22]. (a) Emulating the effect of extracellular Mg^{2+} on NMDA-activated whole-cell currents. The current responses were measured either in presence or absence of Mg^{2+}. The membrane potential was set at -60 mV. (b) Emulating the voltage and concentration dependence of block by extracellular Mg^{2+} on glutamate-activated steady-state $I-V$ relations. The four curves represent steady-state whole-cell $I-V$ relations measured during voltage ramps, in the absence of extracellular Mg^{2+} (No Mg) and in the presence of different amount of Mg^{2+} (Mg 1–3). Different values for the parameters governing the $\beta(V_{post})$ (Eqn. (5)) mimic Mg^{2+} with different concentrations. (c) Divalent permeability in which the reversal potential shifted when the extracellular solution was changed from high Na^{+} to high Ca^{2+} extracellular solution by changing the value of the synaptic reverse potential parameter (E_{syn}; Eqn. (2)). The shift of reversal potential is configurable and was set to $+20$ mV.

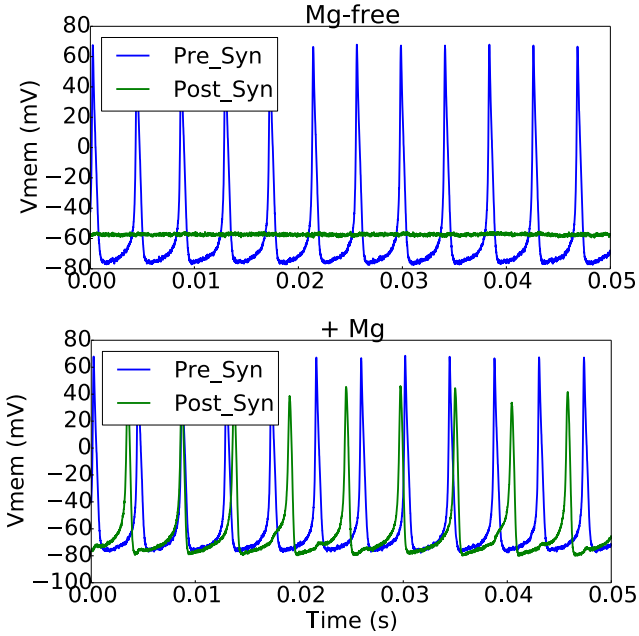

Fig. 4. Effect of an NMDA synapse on the spiking pattern of the postsynaptic neuron. Before 'adding Mg^{2+},' the presynaptic neuron is spiking spontaneously, and the postsynaptic neuron was silent (*top*). After 'adding Mg^{2+},' the postsynaptic neuron is triggered to spike (*bottom*).

of both types of GABA ionotropic receptors and compared their characteristics with GABA receptor responses recorded in different cell models such as $\mathrm{GABA_A}$ receptor chimera expressed in human kidney cells [28] (Fig. 5a) and $\mathrm{GABA_A}$ and $\mathrm{GABA_C}$ responses at synapses in rat retinal bipolar cells [29] (Fig. 5b). The I-V curves for all receptor types were obtained from current measurements at different voltages for different time points corresponding to the application of a voltage pulse (amplitude $=$ 20 mV, duration $=$ 2000 ms) to the presynaptic neuron mimicking GABA releases [28]. Experimental results of the synaptic coupling of two silicons neurons with reciprocal inhibitory $\mathrm{GABA_A}$ synapses were presented in [1].

C. Glycine Receptor

The amino acid glycine is the main inhibitory neurotransmitter in the spinal cord. Similarly to ionotropic GABA receptors, glycine receptors are permeable to Cl^{-} ions and contribute to fast synaptic inhibition [30]. There is a broad variety of glycine receptor subtypes but their electrophysiological characterization remains elusive. Recently, patch clamp recordings showed that the linear I-V curve becomes progressively inwardly-rectifying during desensitization for certain receptor subtypes involved in temporal lobe epilepsy [31]. We decided to emulate receptor

Authorized licensed use limited to: Univ of Calif San Diego. Downloaded on August 06,2021 at 09:57:53 UTC from IEEE Xplore. Restrictions apply.

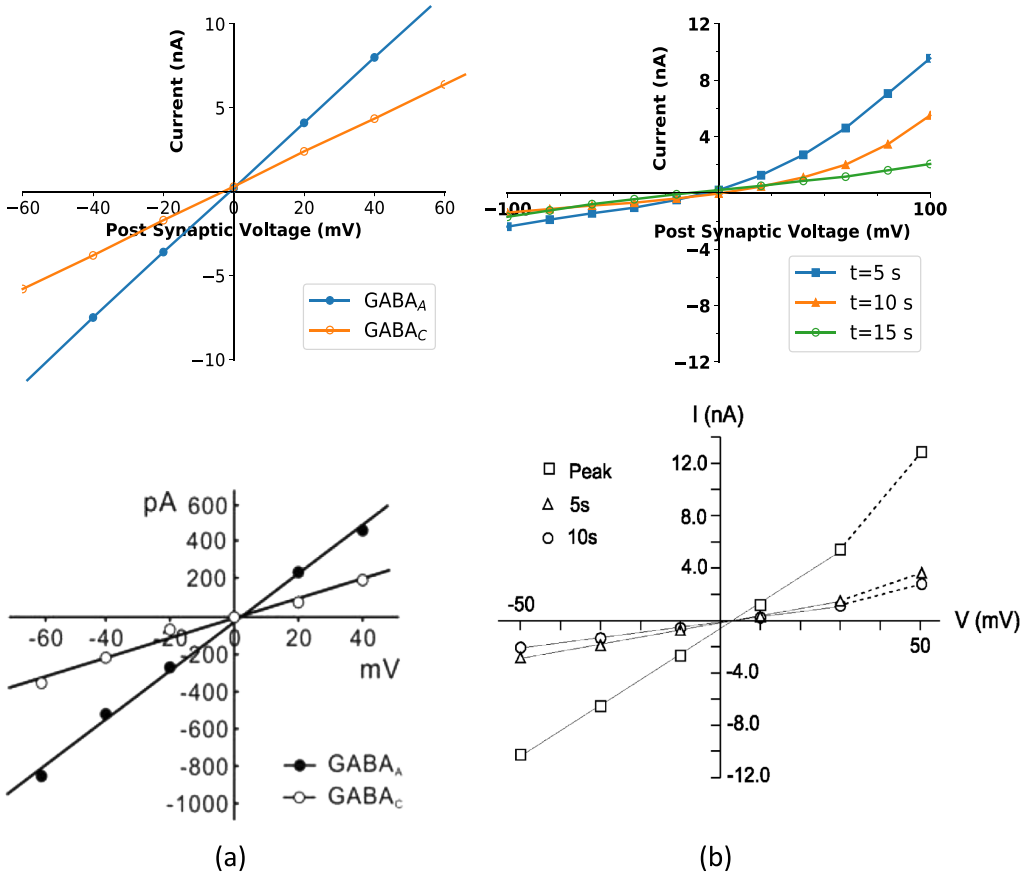

Fig. 5. Characterization of synapses with $\mathrm{GABA_A}$ and $\mathrm{GABA_C}$ receptors. (a) *NeuroDyn* measured I-V curves for the $\mathrm{GABA_A}$ and $\mathrm{GABA_C}$ receptors (*top*) as observed in dissociated rat retinal bipolar cells (*bottom*) [29]. (b) Current-voltage relation for the emulated $\mathrm{GABA_A}$ receptor (*top*) as observed in rat $\mathrm{GABA_A}$ receptors composed of the $\alpha 1\beta 3\gamma 2L$ subunits expressed in HEK293 T cells (*bottom*) [28]. The I-V curve was derived from current measurements at three time points: 5, 10, and 15 seconds. The application of GABA was elicited by applying a 2000 ms voltage pulse of 20 mV to the presynaptic neuron.

desensitization because it is a fundamental property of most ligand-gated ionotropic receptors –limiting current flow after transitioning to a ligand-bound closed state following a prolonged ligand exposure– and can have important physiological consequences by altering the neuron firing activity. Fig. 6 shows the progressive rectification of the glycine current obtained by modifying the opening and closing gate parameters.

D. Postsynaptic Membrane Dynamics

We characterized the postsynaptic membrane dynamics upon activation with a presynaptic action potential. These dynamics are controlled in *NeuroDyn* through adjusting the receptor time constant τ_r through their dependence on presynaptic and postsynaptic potentials as $\tau_r = 1/(\alpha_r(V_{pre}) + \beta_r(V_{post}))$. Excitatory postsynaptic potentials (EPSPs) and inhibitory postsynaptic potentials (IPSPs) evoked by the different receptor types are shown in Fig. 7. As expected from the I-V curves, EPSPs evoked by the different AMPA receptor subtypes had different amplitudes and were maximal for the type I. Similarly, IPSPs evoked by the different GABA receptor subtypes had different amplitudes and was maximal for the $\mathrm{GABA_A}$ subtype. For the glycine receptor, we used a linear I-V curve as shown in Fig. 6. The longer time constant of the NMDA receptor EPSP was obtained by adjusting the closing rate $\beta(r)$ to decrease substantially with increasing postsynaptic potential values.

IV. Electrical Synapses

Electrical synapses are formed by gap junctions between adjacent neurons in both vertebrates and invertebrates [5], [32]. Contrary to chemical synapses, most of the electrical synapses operate in analog mode and allow the nearly ohmic bidirectional passage of current and small metabolites between the connected neurons. This bidirectional form of analog signaling enable populations of neurons to rapidly share and propagate voltage changes among them. Theoretical and experimental evidence indicate that electrical synapses have both excitatory and inhibitory effects [4], can enhance the signal-to-noise ratio [33], and contribute to patterns of network activity including synchronization and oscillations [34]–[37]. We implemented bidirectional (symmetric) electrical synapses in two different ways. In *NeuroDyn*, the trivial solution to allow the bidirectional passage of current between two silicon neurons is to connect their membrane voltage pins through an external resistance wire. *NeuroDyn* further permits more general, biophysical forms of

Authorized licensed use limited to: Univ of Calif San Diego. Downloaded on August 06,2021 at 09:57:53 UTC from IEEE Xplore. Restrictions apply.

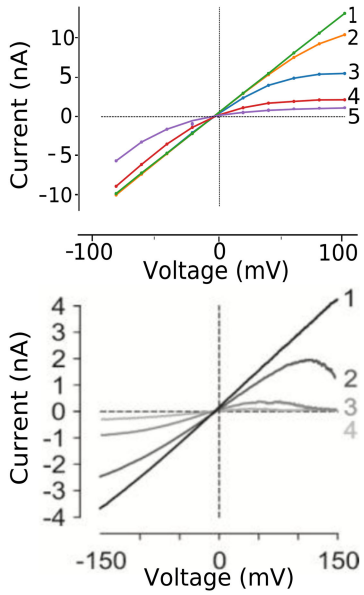

Fig. 6. *NeuroDyn* characterization of synapses with glycine receptors. *Top,* the I-V curves at peak are linear and become progressively inwardly rectifying upon receptor desensitization. The different colors correspond to different values of the opening α_r and closing β_r gate parameters. *Bottom,* current desensitization of a homomeric glycine receptor composed of GlyR α3L subunits at different time points (1–4) in response to 1 mM glycine, reproduced from [31]. The time point 1 corresponds to the linear response at peak.

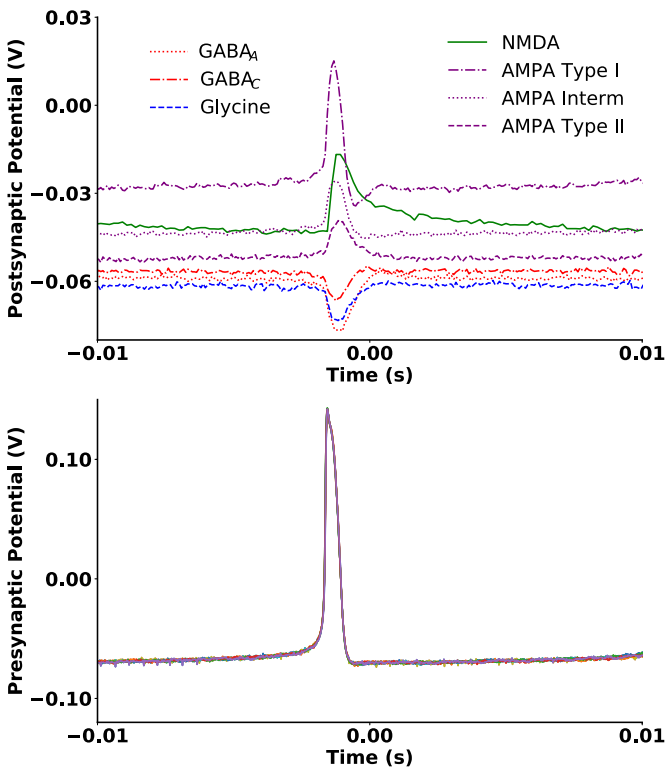

Fig. 7. Measured postsynaptic membrane dynamics. Various types of chemical synapses were activated by a presynaptic action potential (*bottom*), evoking excitatory postsynaptic potentials (EPSPs) for the AMPA receptor subtypes (purple lines) and NMDA receptors (green solid line), and inhibitory postsynaptic potentials (IPSPs) for the GABA receptor subtypes (red lines) and glycine receptor (blue line).

electrical synapses with voltage-gated conductance by modifying the synaptic current (2) such that the voltage difference driving the synaptic current is between the membrane voltages of the pre- and postsynaptic neurons, i.e.

$$I_{Syn}(t) = g_{syn}\ r(t)\ (V_{post}(t) - V_{pre}(t)) \tag{8}$$

modeling first-order kinetics in gap junctions in rat Schwann cells (glia cells) [38]. Fig. 8 shows the effect of voltage-gated electrical synapses on the neural activity of an all-to-all network of four silicon neurons. Without activating the electrical synapses ($g_{syn} = 0$), the four identically tuned neurons showed no dynamical coupling, firing independently and asynchronously due to jitter induced by noise and device mismatch. In the presence of electrical synapses, the neurons displayed synchronous membrane voltage fluctuations and fired in phase. Similar, but not identical, firing dynamics could be achieved for two silicon neurons by tuning the governing parameters to compensate for device mismatch. However, this does alleviate the effect of phase noise in desynchronizing the dynamics of the two neurons.

V. Discussion

In this work, we emulated in neuromorphic VLSI hardware the current-voltage (I-V) characteristics of the main ionotropic receptors present at excitatory, inhibitory, and electrical synapses. In addition to the classic, linear, fast AMPA-like excitatory and $\mathrm{GABA_A}$-like inhibitory synapses generally implemented on neuromorphic hardware [16], we also emulated postsynaptic currents from NMDA, $\mathrm{GABA_C}$, and glycine receptors, as well as two other AMPA receptor sub-types with different rectifying properties. Voltage-dependent ionic currents were described by a first-order Markov kinetic model of the receptor channel and the sign of a chemical synapse could easily be configured by the polarity of the reversal potential. Using programmable opening and closing channel rate functions, we implemented neuromorphic synapses with receptors exhibiting different kinetic properties and I-V relationships, including linear (Fig. 5a), inward (Fig. 6), and outward (Fig. 3b) rectifications. By independently modulating the spline functions of the opening and closing rates of *NeuroDyn*, it should be straightforward to implement the postsynaptic current of the other main ionotropic receptors present in the central and peripheral nervous systems, including the serotonin type 3 ($\mathrm{5\text{-}HT_3}$) receptor which has an I-V curve similar to that of the intermediate AMPA receptor sub-type [39], the neuronal nicotinic acetylcholine receptor which has a linear I-V curve exhibiting strong inward rectification [40], the ATP-gated P2X receptor cation channel family which have a mostly linear I-V relationships with slight amounts of rectification [41], and the transient receptor potential (TRP) cation channels which have a voltage dependence similar to the NMDA receptor [42]. Although the *NeuroDyn* kinetic model has only two states (open and closed), it provides a great flexibility for the emulation of the I-V properties of additional desensitized states as we showed for a class of glycine receptors (Fig. 6). By dynamically reconfiguring the parameters of the spline sigmoidal functions, we were able to simulate the

Authorized licensed use limited to: Univ of Calif San Diego. Downloaded on August 06,2021 at 09:57:53 UTC from IEEE Xplore. Restrictions apply.

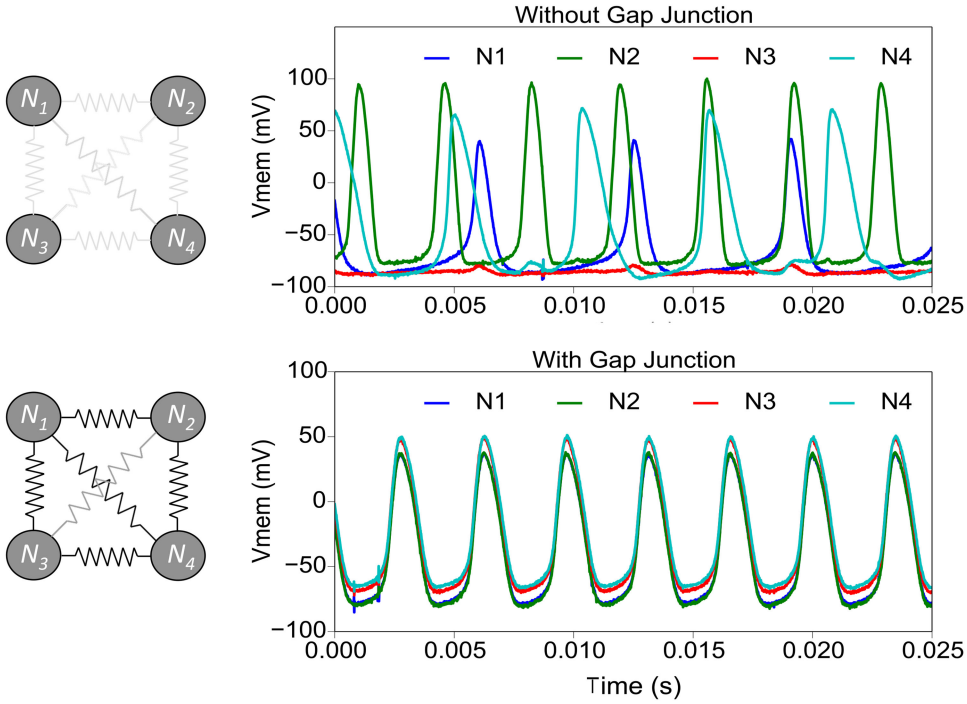

Fig. 8. Electrical synapses and synchronization of neural network activity in *NeuroDyn*. *Top,* in the absence of electrical synapses, four unconnected silicon neurons have independent firing dynamics. *Bottom,* connecting the silicons neurons with voltage-dependent electrical synapses (g_{syn} = 100 μS and $r = 1$) promotes synchronous firing of the four coupled silicon neurons.

desensitization dynamics. A more accurate modeling of receptor desensitization could be achieved with kinetic models having more than two conformational states [43]. In general, a better estimation and configuration of the *NeuroDyn* parameters can be achieved using data assimilation from intracellular neural recordings of the receptor and ionic current(s) of interest [21].

Besides fast excitatory and inhibitory synapses, the NMDA receptor is the only other ionotropic receptor that has received a significant amount of interest in the neuromorphic community. Some authors have developed neuromorphic circuits of the NMDA receptor present outside the synaptic cleft and in dendrites. Irizzary-Valle and Parker designed and simulated a model of extrasynaptic NMDA receptor activated by astrocytes during neural synchronization in a tripartite neuromorphic synapse [44]. Schemmel and colleagues proposed a neuromophic NMDA channel model for emulating dendritic NMDA plateau potentials in a multicompartment neuron circuit [45], [46]. Other authors reproduced the voltage dependence and slower kinetic of the NMDA receptor and used them as coincidence detectors for the implementation of synaptic learning rules [47], [48]. Bartolozzi and Indiveri described a NMDA circuit that could emulate short- and long-term plasticity when connected to other circuit modules [47]. This circuit was later implemented on a neuromorphic chip with hundreds of silicon neurons and on-line learning capabilities [49]–[51]. In that neuromorphic chip, the nonlinear conductance dynamics resulted from adaptive and learning features such as spike-frequency adaptation and bi-stable plastic synapses. Using a more complex synaptic model, Rachmuth and colleagues implemented a neuromorphic synapse circuit able to reproduce both rate- and spike-time-dependent plasticity learning rules [48]. In that synaptic model, NMDA receptors acted as coincidence detectors at both the pre- and postsynaptic sites. Postsynaptic site contained both AMPA and NMDA receptors as well as an additional circuit for modeling intracellular calcium signal. Presynaptic site contained NMDA and CB1 receptors as well as intracellular calcium signals. Overall, these different hardware implementations of the NMDA receptor typically require additional circuit blocks. One of the main advantages of our approach is that the reconfigurable architecture of *NeuroDyn* provides a versatile platform to implement a variety of synapse types in biophysical terms of ionotropic receptors, with programmable DACs that scale to deep-submicron CMOS technologies, and without the need for additional analog circuit blocks. In *NeuroDyn*, power consumption scales linearly with the number of neurons and the numbers of synapses, in particular with the number of gating variables and conductances. Power consumption and bandwidth can be traded, also with linear trade-off, through global tuning of bias currents scaling all conductances and rate constants in the model.

Increasing the variety of synapse types in neuromorphic hardware is critical for at least two distinct applications at different levels of organization. At the single neuron level, a greater synaptic heterogeneity will provide more flexibility for interfacing biological and silicon neurons through artificial synapses in dynamic clamp applications using neural models implemented in VLSI hardware [17], [18], [52]–[54]. In particular, our implementation of glycinergic synapses would enable connecting silicon neurons with neurons in the spinal cord where glycine acts

Authorized licensed use limited to: Univ of Calif San Diego. Downloaded on August 06,2021 at 09:57:53 UTC from IEEE Xplore. Restrictions apply.

as the main inhibitory neurotransmitter [55]. Similarly, our implementation of bidirectional electrical synapses would enable dynamic clamp applications of a large variety of circuits where gap junctions are present. This would prove particularly useful to dissect the contribution of chemical and electrical synaptic transmission in mixed chemical-artificial synapses where gap junctions are present at the synaptic terminal next to synaptic vesicles and postsynaptic density [56], [57]. These mixed chemical/electrical synapses have only been found at glutamatergic axon terminals and their role still remains obscure (for a recent review, see [58]). However, the current version of *NeuroDyn* does not allow the emulation of asymmetric electrical synapses which let current preferentially pass in one direction. Further work is necessary as the extent of rectification can have subtle computational effects that can significantly alter network activity [59], [60]. At the population level, neuromorphic synapses expressing different types of receptors are required for the emulation of biologically realistic neural network models with complex dynamics. Neuromorphic platforms for the simulation of large-scale neural networks up to a million of neurons are now available in digital and mixed analog-digital VLSI hardware [61]. As emerging CMOS-compatible memristive devices [62] will soon enable the emulation of large-scale neural network models on neuromorphic VLSI hardware with a number of neurons, and synapses, similar to their biological counterparts, it is essential to design and implement neuromorphic circuits taking into account the functional heterogeneity and complex spatiotemporal dynamics of biological synapses. In addition, the immense number of neurons and synapses in these emerging new hardware platforms will require systematical parameter estimation approaches, such as data assimilation methods [21] and their extensions, and means for implementing synaptic plasticity innately in the neuromorphic circuits [63].

VI. Conclusion

In this work, we presented the implementation and characterization of diverse synapse types on neuromorphic VLSI hardware. We focused on the emulation of the current-voltage characteristics of the main ionotropic receptors present at excitatory and inhibitory synapses, as well as in gap junctions present in electrical synapses. By dynamically reconfiguring the opening and closing rates parameters, we also emulated the temporal dynamics of EPSPs, IPSPs, and receptor desensitization. As theoretical and experimental neuroscience continue to reveal the extraordinary complexity of biological synapses, further work is needed for the design and implementation of neuromorphic synapses endowed with a larger temporal dynamic range, including the slower dynamics of metabotropic and perisynaptic receptors, retrograde messengers, receptor desensitization, neuromodulation, and receptor trafficking to name but a few. A greater heterogeneity of synapse types and synaptic dynamics would be advantageous both for large-scale neurmorphic computing and for neuromorphic neural interfaces between silicon and biological neurons.

References

[1] T. Yu and G. Cauwenberghs, "Analog VLSI biophysical neurons and synapses with programmable membrane channel kinetics," *IEEE Trans. Biomed. Circuits Syst.*, vol. 4, no. 3, pp. 139–148, Jun. 2010.

[2] T. Yu, T. J. Sejnowski, and G. Cauwenberghs, "Biophysical neural spiking, bursting, and excitability dynamics in reconfigurable analog VLSI," *IEEE Trans. Biomed. Circuits Syst.*, vol. 5, no. 5, pp. 420–429, Oct. 2011.

[3] J. Gjorgjieva, G. Drion, and E. Marder, "Computational implications of biophysical diversity and multiple timescales in neurons and synapses for circuit performance," *Current Opinion Neurobiology*, vol. 37, pp. 44–52, 2016.

[4] B. W. Connors, "Synchrony and so much more: Diverse roles for electrical synapses in neural circuits," *Developmental Neurobiology*, vol. 77, pp. 610–624, 2017.

[5] J. I. Nagy, A. E. Pereda, and J. E. Rash, "Electrical synapses in mammalian CNS: Past eras, present focus and future directions," *Biochimica Biophysica Acta*, vol. 1860, no. 1, pp. 102–123, 2018.

[6] A. M. Craig and H. Boudin, "Molecular heterogeneity of central synapses: Afferent and target regulation," *Nature Neuroscience*, vol. 4, no. 6, 2001, Art. no. 569.

[7] J. Lisman, "Glutamatergic synapses are structurally and biochemically complex because of multiple plasticity processes: Long-term potentiation, long-term depression, short-term potentiation and scaling," *Philos. Trans. R. Soc. B*, vol. 372, no. 1715, 2017, Art. no. 20160260.

[8] E. R. Kandel *et al.*, *Principles of Neural Science*. New York, NY, USA: McGraw-Hill, 2000, vol. 4.

[9] C. Koch and G. Laurent, "Complexity and the nervous system," *Science*, vol. 284, no. 5411, pp. 96–98, 1999.

[10] J. Lengler, F. Jug, and A. Steger, "Reliable neuronal systems: The importance of heterogeneity," *PLoS One*, vol. 8, no. 12, 2013, Art. no. e80694.

[11] V. Balasubramanian, "Heterogeneity and efficiency in the brain," *Proc. IEEE*, vol. 103, no. 8, pp. 1346–1358, Aug. 2015.

[12] M. Shamir and H. Sompolinsky, "Implications of neuronal diversity on population coding," *Neural Comput.*, vol. 18, no. 8, pp. 1951–1986, 2006.

[13] M. I. Chelaru and V. Dragoi, "Efficient coding in heterogeneous neuronal populations," *Proc. Nat. Acad. Sci. USA*, vol. 105, pp. 16344–16349, 2008.

[14] K. Padmanabhan and N. N. Urban, "Intrinsic biophysical diversity decorrelates neuronal firing while increasing information content," *Nature Neuroscience*, vol. 13, no. 10, 2010, Art. no. 1276.

[15] A. Pavasović, A. G. Andreou, and C. R. Westgate, "Characterization of subthreshold MOS mismatch in transistors for VLSI systems," *J. VLSI Signal Process. Syst. Signal, Image, Video Technol.*, vol. 8, no. 1, pp. 75–85, 1994.

[16] P. A. Merolla *et al.*, "A million spiking-neuron integrated circuit with a scalable communication network and interface," *Science*, vol. 345, pp. 668–673, 2014.

[17] G. L. Masson *et al.*, "Feedback inhibition controls spike transfer in hybrid thalamic circuits," *Nature*, vol. 417, pp. 854–858, 2002.

[18] A. Prinz, L. F. Abbott, and E. Marder, "The dynamic clamp comes of age," *Trends Neuroscience*, vol. 27, pp. 218–224, 2004.

[19] J. Wang *et al.*, "Neuromorphic synapses with reconfigurable voltage-gated dynamics for biohybrid neural circuits," in *Proc. IEEE Biomed. Circuits Syst. Conf.*, Oct. 2017, pp. 1–4.

[20] S.-I. Itazawa, T. Isa, and S. Ozawa, "Inwardly rectifying and Ca^{2+}-permeable AMPA-type glutamate receptor channels in rat neocortical neurons," *J. Neurophysiology*, vol. 78, no. 5, pp. 2592–2601, 1997.

[21] J. Wang *et al.*, "Assimilation of biophysical neuronal dynamics in neuromorphic VLSI," *IEEE Trans. Biomed. Circuits Syst.*, vol. 11, no. 6, pp. 1258–1270, Dec. 2017.

[22] H. Monyer *et al.*, "Heteromeric NMDA receptors: Molecular and functional distinction of subtypes," *Science*, vol. 256, no. 5060, pp. 1217–1221, 1992.

[23] M. S. Washburn *et al.*, "Differential dependence on GluR2 expression of three characteristic features of AMPA receptors," *J. Neuroscience*, vol. 17, no. 24, pp. 9393–9406, 1997.

[24] M. Mayer and G. Westbrook, "Permeation and block of n-methyl-d-aspartic acid receptor channels by divalent cations in mouse cultured central neurones," *J. Physiol.*, vol. 394, no. 1, pp. 501–527, 1987.

[25] D. R. Curtis and G. A. Johnston, "Amino acid transmitters in the mammalian central nervous system," *Ergebnisse Physiologie Reviews Physiol*, vol. 69, pp. 97–188, 1974.

[26] A. Maffei *et al.*, "Emerging mechanisms underlying dynamics of GABAergic synapses," *J. Neuroscience*, vol. 37, no. 45, pp. 10792–10799, 2017.

Authorized licensed use limited to: Univ of Calif San Diego. Downloaded on August 06,2021 at 09:57:53 UTC from IEEE Xplore. Restrictions apply.

[27] H. Qian and J. E. Dowling, "GABAA and GABAC receptors on hybrid bass retinal bipolar cells," *J. Neurophysiology*, vol. 74, no. 5, pp. 1920–1928, 1995.
[28] M. T. Bianchi and R. L. Macdonald, "Slow phases of GABA(A) receptor desensitization: Structural determinants and possible relevance for synaptic function," *J. Physiol.*, vol. 544, no. Pt 1, pp. 3–18, 2002.
[29] Y.-C. Yu, L.-H. Cao, and X.-L. Yang, "Modulation by brain natriuretic peptide of GABA receptors on rat retinal on-type bipolar cells," *J. Neuroscience*, vol. 26, no. 2, pp. 696–707, 2006.
[30] P. Legendre, "The glycinergic inhibitory synapse," *Cellular Mol. Life Sci.*, vol. 58, no. 5/6, pp. 760–793, 2001.
[31] C. Raltschev *et al.*, "Electrophysiological signature of homomeric and heteromeric glycine receptor channels," *J. Biol. Chem.*, vol. 291, no. 34, pp. 18030–18040, 2016.
[32] B. W. Connors and M. A. Long, "Electrical synapses in the mammalian brain," *Annu. Rev. Neurosci.*, vol. 27, pp. 393–418, 2004.
[33] S. H. DeVries *et al.*, "Electrical coupling between mammalian cones," *Current Biol.*, vol. 12, no. 22, pp. 1900–1907, 2002.
[34] I. Van Welie *et al.*, "Conditional spike transmission mediated by electrical coupling ensures millisecond precision-correlated activity among interneurons in vivo," *Neuron*, vol. 90, no. 4, pp. 810–823, 2016.
[35] S. Trenholm *et al.*, "Intrinsic oscillatory activity arising within the electrically coupled AII amacrine-ON cone bipolar cell network is driven by voltage-gated Na^+ channels," *J. Physiol.*, vol. 590, no. 10, pp. 2501–2517, 2012.
[36] M. V. Bennett and R. S. Zukin, "Electrical coupling and neuronal synchronization in the mammalian brain," *Neuron*, vol. 41, no. 4, pp. 495–511, 2004.
[37] M. Nomura, T. Fukai, and T. Aoyagi, "Synchrony of fast-spiking interneurons interconnected by GABAergic and electrical synapses," *Neural Comput.*, vol. 15, no. 9, pp. 2179–2198, 2003.
[38] M. Chanson *et al.*, "Gating characteristics of a steeply voltage-dependent gap junction channel in rat schwann cells," *J. Gen. Physiol.*, vol. 102, no. 5, pp. 925–946, 1993.
[39] N. K. McKinnon, D. C. Reeves, and M. H. Akabas, "5-HT3 receptor ion size selectivity is a property of the transmembrane channel, not the cytoplasmic vestibule portals," *J. Gen. Physiol.*, vol. 138, no. 4, pp. 453–466, 2011.
[40] A. P. Haghighi and E. Cooper, "Neuronal nicotinic acetylcholine receptors are blocked by intracellular spermine in a voltage-dependent manner," *J. Neuroscience*, vol. 18, no. 11, pp. 4050–4062, 1998.
[41] B. S. Khakh *et al.*, "Neuronal P2X transmitter-gated cation channels change their ion selectivity in seconds," *Nature Neuroscience*, vol. 2, no. 4, 1999, Art. no. 322.
[42] C. Strübing *et al.*, 'TRPC1 and TRPC5 form a novel cation channel in mammalian brain," *Neuron*, vol. 29, no. 3, pp. 645–655, 2001.
[43] A. Destexhe, Z. F. Mainen, and T. J. Sejnowski, "Kinetic models of synaptic transmission," *Methods Neuronal Model.*, vol. 2, pp. 1–25, 1998.
[44] Y. Irizarry-Valle and A. C. Parker, "An astrocyte neuromorphic circuit that influences neuronal phase synchrony," *IEEE Trans. Biomed. Circuits Syst.*, vol. 9, no. 2, pp. 175–187, Apr. 2015.
[45] J. Schemmel *et al.*, "An accelerated analog neuromorphic hardware system emulating NMDA-and calcium-based non-linear dendrites," in *Proc. Neural Netw. Int. Joint Conf.*, 2017, pp. 2217–2226.
[46] S. A. Aamir *et al.*, "A mixed-signal structured AdEx neuron for accelerated neuromorphic cores," *IEEE Trans. Biomed. Circuits Syst.*, vol. 12, no. 5, pp. 1027–1037, Oct. 2018.
[47] C. Bartolozzi and G. Indiveri, "Synaptic dynamics in analog VLSI," *Neural Comput.*, vol. 19, no. 10, pp. 2581–2603, 2007.
[48] G. Rachmuth *et al.*, "A biophysically-based neuromorphic model of spike rate-and timing-dependent plasticity," *Proc. Nat. Acad. Sci. USA*, vol. 108, no. 49, pp. E1266–E1274, 2011.
[49] E. Chicca *et al.*, "Neuromorphic electronic circuits for building autonomous cognitive systems," *Proc. IEEE*, vol. 102, no. 9, pp. 1367–1388, Sep. 2014.
[50] N. Qiao *et al.*, "A reconfigurable on-line learning spiking neuromorphic processor comprising 256 neurons and 128K synapses," *Frontiers Neuroscience*, vol. 9, 2015, Art. no. 141.
[51] S. Moradi *et al.*, "A scalable multicore architecture with heterogeneous memory structures for dynamic neuromorphic asynchronous processors (dynaps)," *IEEE Trans. Biomed. Circuits Syst.*, vol. 12, no. 1, pp. 106–122, Feb. 2018.
[52] G. L. Masson, S. L. Masson, and M. Moulins, "From conductances to neural network properties: Analysis of simple circuits using the hybrid network method," *Prog. Biophys. Mol. Biol.*, vol. 64, pp. 201–220, 1995.
[53] S. L. Masson *et al.*, "Analog circuits for modeling biological neural networks: Design and applications," *IEEE Trans. Biomed. Eng.*, vol. 46, no. 6, pp. 638–645, Jun. 1999.
[54] M. Sorensen *et al.*, "Using a hybrid neural system to reveal regulation of neuronal network activity by an intrinsic current," *J. Neuroscience*, vol. 24, pp. 5427–5438, 2004.
[55] D. Curtis, L. Hösli, G. Johnston, and I. Johnston, "The hyperpolarization of spinal motoneurones by glycine and related amino acids," *Exp. Brain Res.*, vol. 5, no. 3, pp. 235–258, 1968.
[56] C. Sotelo and H. Korn, "Morphological correlates of electrical and other interactions through low-resistance pathways between neurons of the vertebrate central nervous system," *Int. Rev. Cytology*, vol. 55, pp. 67–107, 1978.
[57] A. E. Pereda, "Electrical synapses and their functional interactions with chemical synapses," *Nature Rev. Neuroscience*, vol. 15, no. 4, pp. 250–263, 2014.
[58] J. I. Nagy, A. E. Pereda, and J. E. Rash, "On the occurrence and enigmatic functions of mixed (chemical plus electrical) synapses in the mammalian CNS," *Neuroscience Lett.*, vol. 16, pp. 53–64, 2017.
[59] E. Marder, "Electrical synapses: Beyond speed and synchrony to computation," *Current Biol.*, vol. 8, no. 22, pp. R795–R797, 1998.
[60] G. J. Gutierrez and E. Marder, "Rectifying electrical synapses can affect the influence of synaptic modulation on output pattern robustness," *J. Neuroscience*, vol. 33, no. 32, pp. 13238–13248, 2013.
[61] S. Furber, "Large-scale neuromorphic computing systems," *J. Neural Eng.*, vol. 13, 2016, Art. no. 051001.
[62] S. Hamdioui *et al.*, "Memristor for computing: Myth or reality?" in *Proc. Conf. Des., Autom., Test Eur., Conf. Exhib.*, 2017, pp. 722–731.
[63] G. Cauwenberghs, "Reverse engineering the cognitive brain," *Proc. Nat. Acad. Sci. USA*, vol. 110, pp. 15512–15513, 2013.

Authorized licensed use limited to: Univ of Calif San Diego. Downloaded on August 06,2021 at 09:57:53 UTC from IEEE Xplore. Restrictions apply.